

COMPLEX FORMATION OF TRANSITION ELEMENT IMPURITIES IN SILICON

C.A.J. AMMERLAAN and A.B. VAN OOSTEN

Natuurkundig Laboratorium der Universiteit van Amsterdam, Valckenierstraat 65, NL-1018 XE Amsterdam, The Netherlands

Very recently a number of new impurity complexes in silicon have been identified and characterised in studies by magnetic resonance. The complexes involve transition elements of the 3d, 4d and 5d series. Among the recent findings are the basic structure of substitutional isolated nickel, several iron-acceptor complexes, and impurity pairs with chromium, manganese, copper, palladium or platinum as a constituent. The electron paramagnetic resonance spectrum provides a set of data which allows an unambiguous identification of these centres. Besides, the analysis of the Zeeman energy tensors in the spin Hamiltonians describing the resonances gives insight into the physical properties related to both atomic and electronic structure. Analysis reveals the symmetry of the arrangement of atoms in the complexes as well as the true physical value of the electron spin which is related to the charge states of the centres.

1. INTRODUCTION

Due to their generally high solubility, high mobility and electrical amphoteric activity, transition element impurities have an often major effect on the physical properties of silicon. Transition elements readily form pairs or other complexes of various sizes and composition, which are however quite unstable and dissolve again under moderate thermal treatment. Due to these properties, usually endured as malicious, firm control over these impurities is mandatory for reliable silicon technology.

Electron paramagnetic resonance (EPR) is a powerful method for experimental study of these processes. Centres can be unambiguously identified and labeled in a unique way by the parameters following from the spin-Hamiltonian analysis. In addition, the characteristics of the spectra, such as angular dependence and hyperfine splitting, reveal important information on the atomic and electronic structure of the centres. In many cases the atomic configuration of the centre as embedded in the silicon host crystal is derived leading to a unique reliable model. The distribution of the defect electron around its centre as monitored by self and ligand hyperfine interactions gives clues on the electronic wave function. These fundamental

data allow a detailed picture to be extracted of the impurity in the host: its atomic structure and electronic binding.

Research by magnetic resonance has now led to the observation of nearly 300 paramagnetic centres in silicon. A large fraction of these centres, about 75, has an established relation to transition element impurities. The large number again reflects the frequent presence and activity of this class of impurities. Recently several new centres involving transition elements of the 3d, 4d and 5d series, were observed and identified for the first time. This paper will first describe, in section 2, the main aspects of some of these centres as reported recently. This includes the basic substitutional nickel impurity, several pairs and complexes involving iron, and other pairs in which the 4d element palladium or the 5d element platinum are constituents. In section 3 of the paper a special analysis of resonance data is presented using alternative spin Hamiltonians with different values of effective spin. This illustrates the way in which experimental observations through their careful analysis lead to determination of the value of the spin with most physical significance, which is related to the number of spin-coupled electrons in the centre, and hence to its charge state.

2. NEW EPR CENTRES

2.1. Substitutional nickel

Only recently the paramagnetic resonance spectrum of negative substitutional nickel in silicon was reported^{1,2}. Spectra for the similar centres Si:Pd⁻, Si:Pt⁻ and Ge:Ni⁻ are already known for over 25 years^{3,4}. From the data one concludes that the structure of all these centres is very much alike. The angular variation of the resonance fields of Si:Ni⁻ for rotation of the magnetic field in the (0 $\bar{1}1$) plane is shown in figure 1. The principal g-values as given in table I are derived from these measurements. The symmetry of the Si:Ni centre, as for the other centres, is orthorhombic-I. This distortion is consistent with predominant bonding to two of the four silicon atoms on nearest-neighbour positions. A strong approximately $\langle 111 \rangle$ axial hyperfine interaction with these two silicon atoms is observed. After doping with nickel impurity which is enriched in the magnetic isotope, i.e. with ⁶¹Ni with nuclear spin $I=3/2$, the EPR spectrum shows a

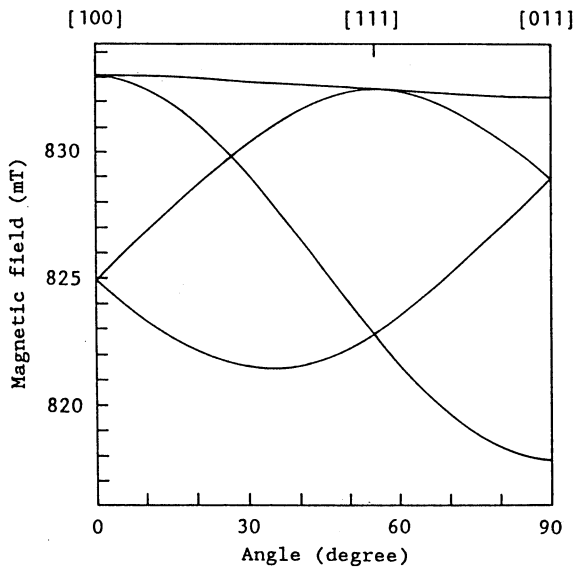


FIGURE 1

Angular dependence of the EPR line positions of the Si:Ni_s spectrum as a function of magnetic field orientation in the (0 $\bar{1}1$) plane, demonstrating orthorhombic-I symmetry of the centre. Microwave frequency $\nu \approx 23$ GHz.

fourfold line structure. This is experimental evidence for the presence of one nickel atom in the centre. The spectrum is shown in figure 2. The new nickel spectrum is only observed in moderately n-type doped material. Preliminary studies of the marked dependence of its intensity on illumination with filtered light were made. Substitutional nickel presumably represents a small fraction only of the total amount of nickel present in the silicon.

2.2. Iron-acceptor pairs

Ion pairing between positively charged ionised iron donors and negatively charged shallow acceptors easily takes place near room temperature due to the high mobility of iron atoms. Several of the pairs were already observed by their characteristic EPR spectra about 30 years ago⁵. By the more recent detection of the iron-aluminium pairs in two atomic configurations^{6,7}, two iron-gallium pairs with atoms on next-nearest position⁷ and the iron-indium pair with atoms on nearest positions^{8,9} the set of available EPR data became quite complete. Sym-

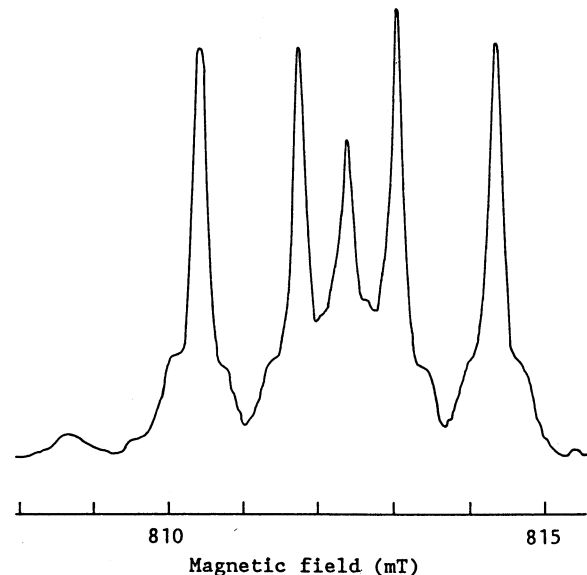


FIGURE 2

Electron paramagnetic resonance spectrum of nickel in silicon showing fourfold splitting due to the isotope nickel-61, enrichment 88%, with nuclear spin $I=3/2$. Magnetic field $\vec{B} \parallel \langle 011 \rangle$.

metries and g -tensor principal values are given in table I. The trigonal centres have the iron atom on a nearest interstitial position in a $\langle 111 \rangle$ direction from the substitutional acceptor. In the orthorhombic pairs the axis between the two impurities is $\langle 100 \rangle$ oriented. Observation of FeB pairs in orthorhombic next-nearest interstitial neighbour position for the iron is still lacking. Identification of the spectra is based on the symmetry revealed by the rotation pattern and hyperfine structure in the spectra arising from magnetic nuclei. For the new FeIn pair figure 3 demonstrates the trigonal symmetry. The presence of one indium atom is shown by the ideally resolved hyperfine interaction with the isotope ^{115}In with nuclear spin $I=9/2$ and natural abundance 95.72%, see figure 4. Some pairs are observed both in the ground state and in spin-orbit excited state. A discussion on the relation between the g -tensors in ground and excited states will be given in the next section. Binding in the pairs has been ascribed to covalent forces¹². The centres

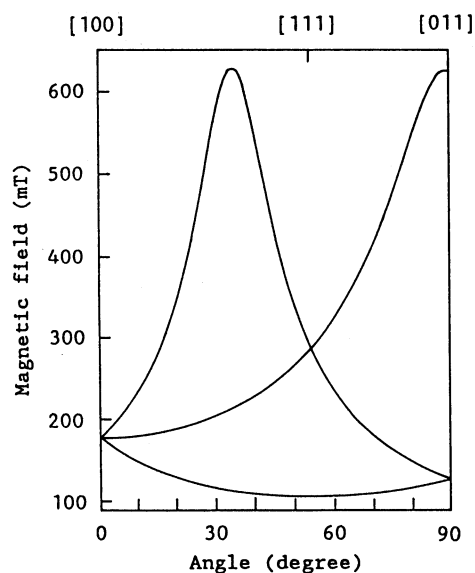


FIGURE 3
Angular dependence of the EPR line positions of the $\text{Si:Fe}_2\text{In}_2$ spectrum as a function of magnetic field orientation in the $(0\bar{1}1)$ plane, demonstrating trigonal symmetry of the centre. Microwave frequency $\nu \approx 9$ GHz.

exhibit bistability due to hopping of the iron atom from the nearest site to the acceptor with trigonal symmetry, to the next further interstitial site with orthorhombic symmetry. In studies of such bistability the binding could be described using ionic forces¹³.

2.3. Iron-iron pair

Directly after a fast quench following iron diffusion into silicon at about 1200°C the EPR spectrum labeled Si-NL24 was observed¹⁴. Its angular dependence, as shown in figure 5, reveals a centre of monoclinic-I symmetry. When analysed with effective spin $S=1/2$ the principal g -values as given in table I are obtained. The unusually high g -value $g_3=9.44$ indicates coupling of several electron spins, suggesting an alternative analysis with a higher value for the spin S . Confirming this complexity, a second monoclinic-I spectrum was observed which is due to resonance in an excited state doublet of the same centre^{15,16}. These g -values, also analysed with $S=1/2$, are included in table I as well. The detailed coherent analysis of both

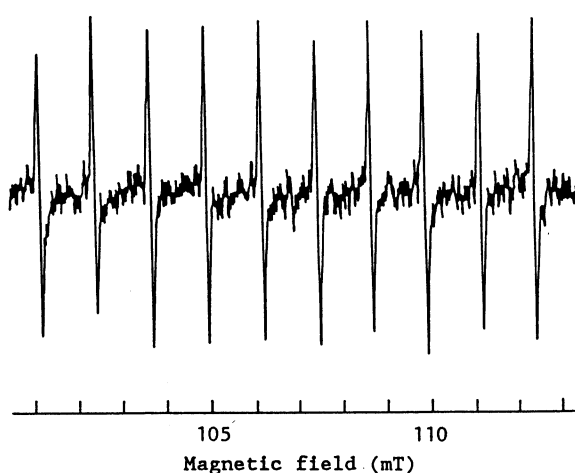


FIGURE 4
Electron paramagnetic resonance spectrum of the trigonal iron-indium pair in silicon showing tenfold splitting due to the isotope indium-115, natural abundance 95.72%, with nuclear spin $I=9/2$. Magnetic field $\vec{B} \parallel \langle 111 \rangle$.

spectra in a spin $S=5/2$ formalism is briefly discussed in section 3 of this paper. After introduction of the magnetic isotope ^{57}Fe , with nuclear spin $I=1/2$, hyperfine structure as indicated in figure 6 is observed. The number of lines in the spectrum and their intensities are unambiguously interpreted as due to two iron atoms, on symmetry-equivalent positions in the NL24 centre. Models consistent with this conclusion and with the observed monoclinic symmetry are discussed in the literature¹⁴. The EPR spectrum is lost by thermal anneal at, or just above, room temperature. This may be interpreted as further iron aggregation at the $(\text{Fe}_i)_2$ centre, leading to larger complexes, of which the $(\text{Fe}_i)_4$ -complex with EPR spectrum NL22 is the only reported species¹⁷.

2.4. Iron-iron-boron complexes

The process of iron precipitation can also proceed via the iron-acceptor complexes. Evidence for such a process was found in boron doped silicon by the observation of two FeFeB-complexes, one with monoclinic-I, the other

with orthorhombic-I symmetry^{15,16,18}. The high g -values, see table I, as well as the observation of resonance in excited state doublets^{15,16}, confirms the high spin of the centres, arising from the presence of two iron atoms. Observation of a fourfold splitting due to the ^{11}B isotope, nuclear spin $I=3/2$, abundance 81.2%, reveals the acceptor atom in the centre. To establish detailed structural models, to distinguish between several conceivable models consistent with the symmetry, further measurements of hyperfine interactions with ^{57}Fe , ^{10}B or ^{11}B , and the surrounding ^{29}Si nuclei are required.

2.5. Manganese- and chromium-copper pairs

After co-diffusion of manganese and copper in silicon, followed by cooling in air, two new trigonal EPR spectra were observed¹⁹. The spectra show the sixfold splitting due to one manganese nucleus (isotope ^{55}Mn , spin $I=5/2$, abundance 100%) and additional fourfold splitting by one copper nucleus (isotopes ^{63}Cu and ^{65}Cu , spin $I=3/2$, total abundance 100%). They are

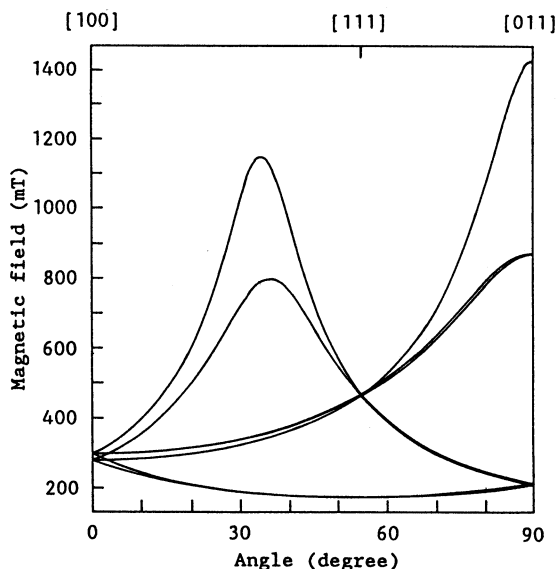


FIGURE 5

Angular dependence of the EPR line positions of the $\text{Si}:(\text{Fe},\text{Fe}_i)^+$ spectrum as a function of magnetic field orientation in the $(0\bar{1}1)$ plane, demonstrating monoclinic-I symmetry of the centre. Microwave frequency $\nu \approx 23$ GHz.

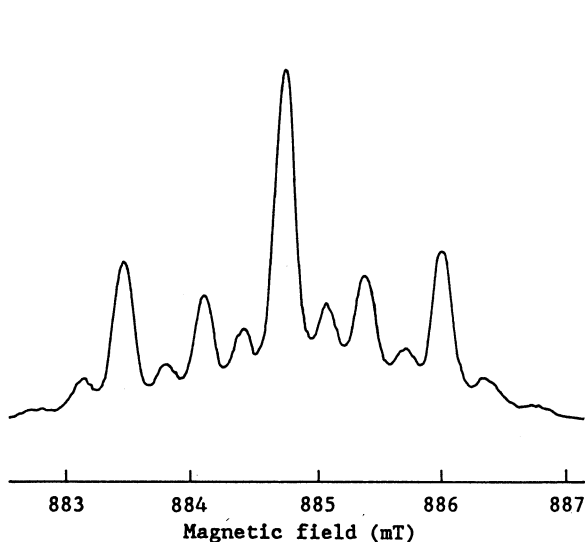


FIGURE 6

Electron paramagnetic resonance spectrum of the iron-iron pair in silicon showing fivefold splitting due to two atoms of the isotope iron-57, enrichment 85%, with nuclear spin $I=1/2$. Magnetic field \vec{B} in the $(0\bar{1}1)$ plane, 75° away from $[100]$.

consequently interpreted as arising from MnCu pairs, with copper on a substitutional site and manganese on a nearest interstitial position. One pair observed in p-type silicon is associated with the MnCu⁺ pair, the other pair observable in n-type silicon then is due to the MnCu⁻ pair. These are the first EPR identified copper-related centres in silicon.

In much the same way, co-diffusion of chromium and copper results in the observation of an EPR spectrum with fourfold splitting due to one copper atom²⁰. The spectrum reveals trigonal symmetry and is interpreted as a neutral Cr_iCu_s pair. The g-tensor components of the three copper-related spectra are given in table I.

2.6. Iron-platinum and iron-palladium pair

In the early work of Ludwig and Woodbury the spectrum Pt(II) was reported³. It was tentatively speculated to be related to a platinum associated with oxygen. However, the spectrum also appeared in oxygen-free float-zone silicon. Presence of iron in the samples strongly

enhanced the Pt(II) signal, while suppressing the well-identified resonance of substitutional Pt⁻. Conclusive evidence for the presence of iron in the Pt(II) centre resulted from doping with ⁵⁷Fe. The spectrum Pt(II) arises from a platinum-iron impurity pair in trigonal arrangement²¹.

A similar trigonal spectrum was observed in palladium diffused crystals²¹. It showed an analogous ⁵⁷Fe hyperfine structure, in addition to the structure arising from ¹⁰⁵Pd. The structure identifies the centre as a pair of one palladium and one iron atom²¹. The principal g-values of both pairs are given in Table I. The parameters of the fine and hyperfine structure of the PtFe and PdFe pairs and their formation conditions are very similar. This indicates a similar structure with presumably the palladium and platinum on a substitutional site and with the iron atom on a nearby <111> interstitial position. By means of deep level transient spectroscopy an electron level associated with the FePd pair was identified²².

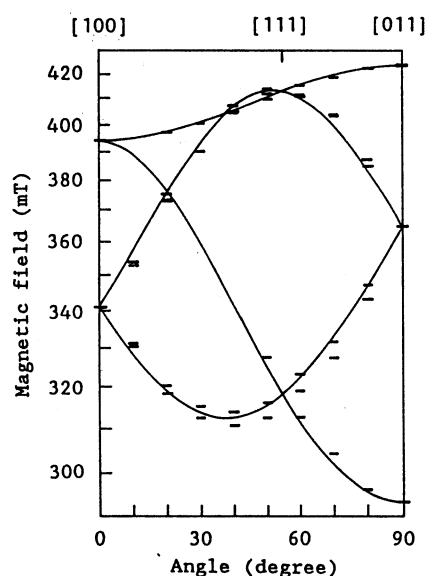


FIGURE 7
Angular dependence of the EPR line positions of the Si:PtPt spectrum as a function of magnetic field orientation in the (0 $\bar{1}1$) plane, demonstrating orthorhombic-I symmetry of the centre. Microwave frequency $\nu \approx 9$ GHz.

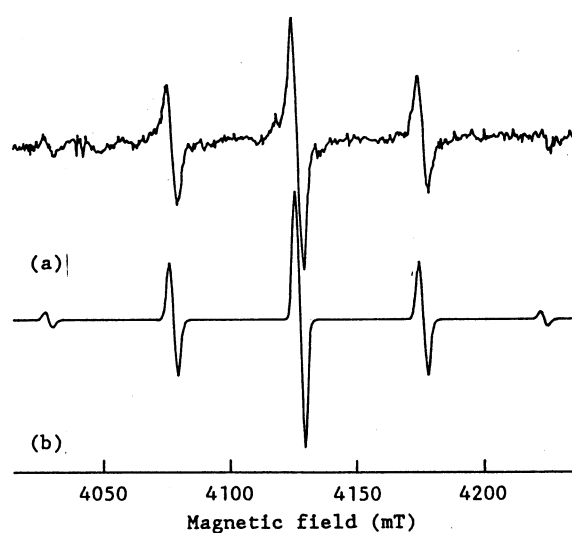


FIGURE 8
Electron paramagnetic resonance spectrum of the platinum-platinum pair in silicon showing five-fold splitting (intensities 3:22:50:22:3) due to two atoms of the isotope platinum-195, natural abundance 33.8%, with nuclear spin $I=1/2$. Magnetic field $\vec{B} \parallel \langle 100 \rangle$. (a) Measured, (b) simulated spectrum.

Table I. Parameters for transition element related centres in silicon.

Spectrum label	Atomic model	Symmetry	Spin S	Principal g-values			g	Reference
				g_1	g_2	g_3		
Lu2	Ni_s^-	Orthorhombic-I	1/2	2.0163	2.0182	2.0536	1.1717	1,2
	$Fe_i In_s$	Trigonal	1/2	6.38	1.08	1.08	2.1868	8,9
	$Fe_i In_s$	Orthorhombic-I	1/2	2.07	3.78	4.40	2.0530	5
NL27	$Fe_i B_s$	Trigonal	1/2	2.0676	4.0904	4.0904	2.0477	10
NL28	$Fe_i Al_s$	Trigonal	1/2	6.389	1.138	1.138	2.1962	6
NL24	$Fe_i Al_s$	Orthorhombic-I	1/2	5.885	1.236	1.612	2.0752	6
	$Fe_i Al_s$	Orthorhombic-I	1/2	1.73	5.36	2.51	2.0554	7
	$Fe_i Ga_s$	Trigonal	1/2	5.089	2.530	2.530	2.0736	11
	$Fe_i Ga_s$	Orthorhombic-I	1/2	6.19	0.59	0.69	2.0854	7
	$Fe_i Ga_s$	Orthorhombic-I	1/2	2.02	4.65	3.37	2.0292	7
	$(Fe_i Fe_i)^+$	Monoclinic-I	1/2	1.15	2.06	9.44	3.2434	14
	$(Fe_i Fe_i)^+$	Monoclinic-I	1/2	3.90	3.50	5.07	2.4305	15,16
NL33	$Fe_i Fe_i B_s$ -complex	Monoclinic-I	1/2	1.472	8.899	2.895	3.1577	15,18
	$Fe_i Fe_i B_s$ -complex	Monoclinic-I	1/2	2.96	3.05	5.46	2.3064	15,16
NL32	$Fe_i Fe_i B_s$ -complex	Orthorhombic-I	1/2	7.902	1.811	4.184	3.0410	15,18
	$Fe_i Fe_i B_s$ -complex	Orthorhombic-I	1/2	1.73	1.94	5.80	2.1186	15,16
	$(Mn_i Cu_s)^+$	Trigonal	3/2	2.0065	2.016	2.016		19
	$(Mn_i Cu_s)^-$	Trigonal	3/2	2.0130	2.025	2.025		19
	$(Cr_i Cu_s)^0$	Trigonal	3/2	2.003	2.0045	2.0045		20
Pt(II)	$Fe_i Pt_s$	Trigonal	1/2	2.0124	2.1264	2.1264	1.2061	3,21
	$Fe_i Pd_s$	Trigonal	1/2	2.0407	2.0887	2.0887	1.1967	21
	PtPt	Orthorhombic-I	1/2	1.6317	1.5181	2.1869	1.0408	23
A27	$FeBV/I$ -complex	Monoclinic-I	1/2	4.78	1.96	3.24	2.0327	24
A28	$FeOV$ -complex	Monoclinic-I	1/2	4.20	2.15	4.10	2.0836	24
NL19	Fe_s^+	Trigonal	3/2	2.1163	2.0935	2.0935		17
NL23	Fe_i -complex	Trigonal	1/2	5.489	2.809	1.768	2.1382	17
NL20	$Fe_i Fe_i V$ -complex	Trigonal	1/2	2.059	6.235	6.235	3.0183	17
NL21	$Fe_i Fe_i V_2$ -complex	Monoclinic-I	1/2	4.90	7.38	1.961	3.0243	17

2.7. Platinum-platinum pair

An EPR spectrum attributed to a platinum-platinum homonuclear pair was observed in float-zone gallium doped silicon, at a measurement temperature of 20 K²³. The identification is based on the observed intensities of hyperfine splitting into 5 lines, proportional to 3:22:50:22:3, see figure 8. This is consistent with two platinum atoms on symmetry-equivalent sites, and the natural abundance 33.8% of the

isotope ¹⁹⁵Pt with nuclear spin I=1/2. From the angular dependence of resonance lines, as given in figure 7, orthorhombic-I symmetry is deduced for the pair. This symmetry is identical to that of the single platinum atom Pt_s^-3 and almost excludes nearest-neighbour sites for the impurity atoms. It could not be concluded whether the platinum atoms are both on substitutional or on interstitial sites. The principal g-values of the pair are in table I.

3. ANALYSIS g-TENSOR

3.1. Kramers doublets

Transition metal elements are characterised by partially filled inner electron shells. Due to exchange coupling between the electrons their spins are aligned. Hund's empirical rule states that maximum spin, consistent with the exclusion principle, is realised as the ground state. For transition elements with more than half-filled shell a description in terms of holes in an otherwise full shell is usually preferable. The degeneracy of the levels in a spin multiplet can be lifted by crystal fields. For an odd number of electrons a twofold degeneracy of Kramers conjugate states will remain. For instance, a spin $S=3/2$ quartet will be split into two doublets; a sextet state formed by spin $S=5/2$ will be split into three doublets in a crystal field of low symmetry. Electron spin resonance can be observed in these Kramers doublets, by splitting the two levels of a doublet in a magnetic field. In case the magnetic field splitting, the Zeeman effect, is small compared to the crystal field splitting such a resonance can be described with adequate accuracy with an effective spin $S=1/2$. The simple spin Hamiltonian which is then applied is

$$\mathcal{H} = +\mu_B \vec{B} \cdot \vec{S}. \quad (1)$$

The results of analysis of spectra with spin $S=1/2$ are given in table I. In nearly all cases the g -values obtained from the analysis deviate strongly from the free-electron value $g=2$. Since in low symmetry one expects orbital contributions to the magnetism to be quenched, these values are unphysical. It indicates that the true spin of the centre is larger than $1/2$. Some of the centres, notably the Cu centres and NL19, can not be analysed, with satisfying accuracy, with spin $1/2$ as the zero field splitting is not large compared to the Zeeman energy. These centres are therefore directly analysed with the more real spin $S=3/2$ and zero-field splitting term.

3.2. Centres with one iron atom

To understand results as given in table I,

it is necessary to establish the relation between g -values in the spin $S=1/2$ formalism and the parameters describing the higher spin multiplet. The interaction between spins is represented by the crystal field term

$$\mathcal{H} = +D(S_z^2 - 5/4) + E(S_x^2 - S_y^2). \quad (2)$$

The first term gives an axial, trigonal or tetragonal, interaction which is chosen along the z -axis. The second term represents an orthorhombic crystal field. For spin $S=3/2$ the basis states are $|-3/2\rangle$, $|-1/2\rangle$, $|+1/2\rangle$ and $|+3/2\rangle$, excluding any orbital effects. With equation (2) and these basis states a matrix $\langle m_S, | \mathcal{H} | m_S \rangle$ can be set up. The energies ϵ_i of the doublets $i=1,2$, obtained by diagonalising the matrix, are given in units of D by

$$\epsilon_i/D = \pm(1+3E^2/D^2)^{1/2}. \quad (3)$$

Wave functions corresponding to these solutions are

$$|\Phi_1\rangle = +\cos\phi|+3/2\rangle + \sin\phi|-1/2\rangle, \quad (4a)$$

$$|\Phi_1^*\rangle = +\cos\phi|-3/2\rangle + \sin\phi|+1/2\rangle, \quad (4b)$$

and

$$|\Phi_2\rangle = -\sin\phi|+3/2\rangle + \cos\phi|-1/2\rangle, \quad (4c)$$

$$|\Phi_2^*\rangle = -\sin\phi|-3/2\rangle + \cos\phi|+1/2\rangle, \quad (4d)$$

with

$$\tan 2\phi = +(E/D)\sqrt{3}. \quad (4e)$$

It is seen that the wave functions entirely depend on the ratio E/D only. To the doublet states the Zeeman energy in an applied magnetic field is treated as a perturbation. This will give accurate results as long as the Zeeman energy is small compared to the separation of the doublets. The g -factor of the electron should now be chosen as the isotropic value of the free electron, $g=2.0023$. To allow some more flexibility, to be discussed below, an adjustable scalar g -value, still close to $g=2$, is introduced into equation (1) for the Zeeman effect, which then becomes

$$\mathcal{H} = +g\mu_B \vec{B} \cdot \vec{S}. \quad (5)$$

Operation of this Hamiltonian on the states $|\Phi_1\rangle$ and $|\Phi_1^*\rangle$, lifting the Kramers degeneracy, will give the splitting observed in the magnetic resonance experiment, which is quantitatively specified by the g -tensor. The result for

Table II. Measured and predicted g-values in the spin S=1/2 formalism for the two doublets (1 and 2) of a true spin 3/2 system. g-Values predicted on the basis of the theory are shown in parenthesis.

Centre	Principal g-values			Scale-factor	Scaled g-values			Dou- blet	E/D
	g_1	g_2	g_3		g_1	g_2	g_3		
FeB	2.0676	4.0904	4.0904	1.0239	2.0194	3.9951	3.9951	2	0.00
trig.	(6.14)	(0.00)	(0.00)		(6.000)	(0.000)	(0.000)	1	
FeAl	6.389	1.138	1.138	1.0981	5.818	1.036	1.036	1	0.18
trig.	(2.00)	(4.29)	(4.29)		(1.819)	(2.878)	(4.940)	2	
FeAl	5.885	1.236	1.612	1.0376	5.672	1.191	1.554	1	0.25
o.rh.	1.73	5.36	2.51	1.0277	1.683	5.215	2.442	2	
FeGa	6.19	0.59	0.69	1.0427	5.936	0.566	0.662	1	0.105
o.rh.	2.02	4.65	3.37	1.0146	1.991	4.583	3.321	2	
FeIn	6.38	1.08	1.08	1.0934	5.835	0.988	0.988	1	0.175
trig.	(2.00)	(4.28)	(4.28)		(1.828)	(2.909)	(2.909)	2	
FeIn	2.07	3.78	4.40	1.0265	2.017	3.628	4.286	2	0.05
o.rh.	(6.14)	(0.31)	(0.30)		(5.985)	(0.306)	(0.291)	1	
NL23	5.489	2.809	1.768	1.0691	5.134	2.627	1.654	2	0.235
	(6.10)	(1.55)	(1.24)		(5.705)	(1.454)	(1.158)	1	
A27	1.96	3.24	4.78	1.0164	1.928	3.188	4.703	2	0.125
	(6.01)	(0.79)	(0.70)		(5.909)	(0.778)	(0.688)	1	
A28	2.15	4.10	4.20	1.0418	2.064	3.935	4.031	2	0.01
	(6.25)	(0.06)	(0.06)		(5.999)	(0.060)	(0.060)	1	

the two doublets is:

$$g_x = g[+2 \pm (+2 - 6E/D) / (1 + 3E^2/D^2)^{1/2}], \quad (6a)$$

$$g_y = g[+2 \pm (+2 + 6E/D) / (1 + 3E^2/D^2)^{1/2}], \quad (6b)$$

$$g_z = g[+2 \mp 4 / (1 + 3E^2/D^2)^{1/2}]. \quad (6c)$$

Also the g-values are a function of the ratio E/D. The result, taking g=2, is illustrated in figure 9 in a plot which is linear in the parameter ϕ . Inspection of this result shows that a g-tensor for doublet 1 and some value ϕ_1 is identical to the g-tensor predicted for doublet 2 for $\phi_2 = 30^\circ - \phi_1$. We restrict ourselves therefore to angles ϕ in the range $0^\circ \leq \phi \leq 15^\circ$. This corresponds to centres which are predominantly axial along the z-axis. Angles near $\phi = 30^\circ$ correspond to centres more axial along the y-axis.

Simple calculation with the results given in equations (6a)-(6c) yields

$$(g_x^2 + g_y^2 + g_z^2)^{1/2} / 3 = g. \quad (7)$$

We therefore calculate this quantity for the experimental data and give the result in table I. Centres which satisfy the criterion g=2 include the iron-acceptor pairs and centres A27, A28 and NL23. Additional criteria, see figure 9, state that one principal value should be between 4 and 6, one other between 0 and 4, and one between 0 and 2. The trigonal FeGa centre does not satisfy the latter requirement and is thus eliminated. Signs of g-values are disregarded. In the experiment signs are not determined; in the theory the signs of perpen-

dicular g -values g_x and g_y have no physical significance. On average over the selected centres the result is remarkably close to $g=2.0700$, which is the g -value for the neutral interstitial iron atom²⁵. To allow for comparison with g -values in the figures, which are drawn for a standard value $g=2$, the experimental values are scaled by division through the factor $g/2$. Results are given in table II and are illustrated in figure 10, plotted linearly versus E/D in the range $0 \leq E/D \leq 1/3$ ($0^\circ \leq \phi \leq 15^\circ$) of axially closest to the z -direction. An excellent match is obtained for the 9 centres selected. The orthorhombic FeAl and FeGa pairs are observed in both doublets. For the other centres the g -tensor for observation in one doublet only is thus far available. On the basis of the theoretical analysis a prediction may now

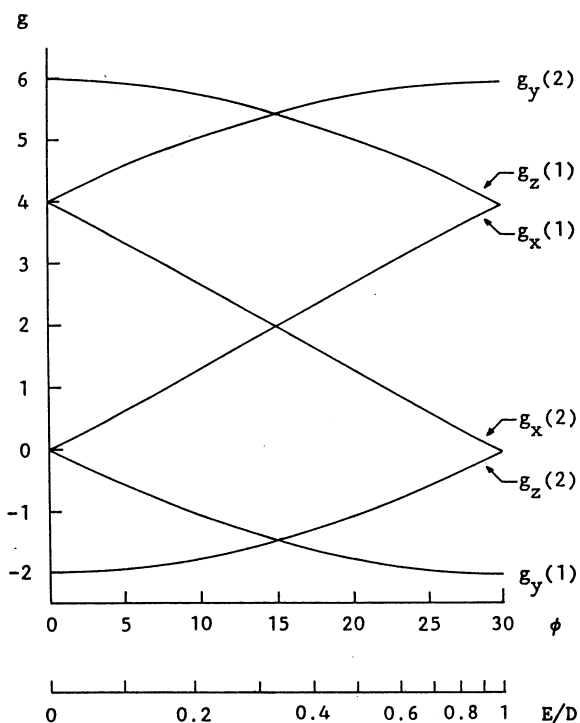


FIGURE 9
Theoretical principal values g_x , g_y and g_z of the g -tensor in the spin $S=1/2$ formalism for the doublets (1) and (2) of a true spin $S=3/2$ system as a function of the ratio E/D of orthorhombic to axial crystal field.

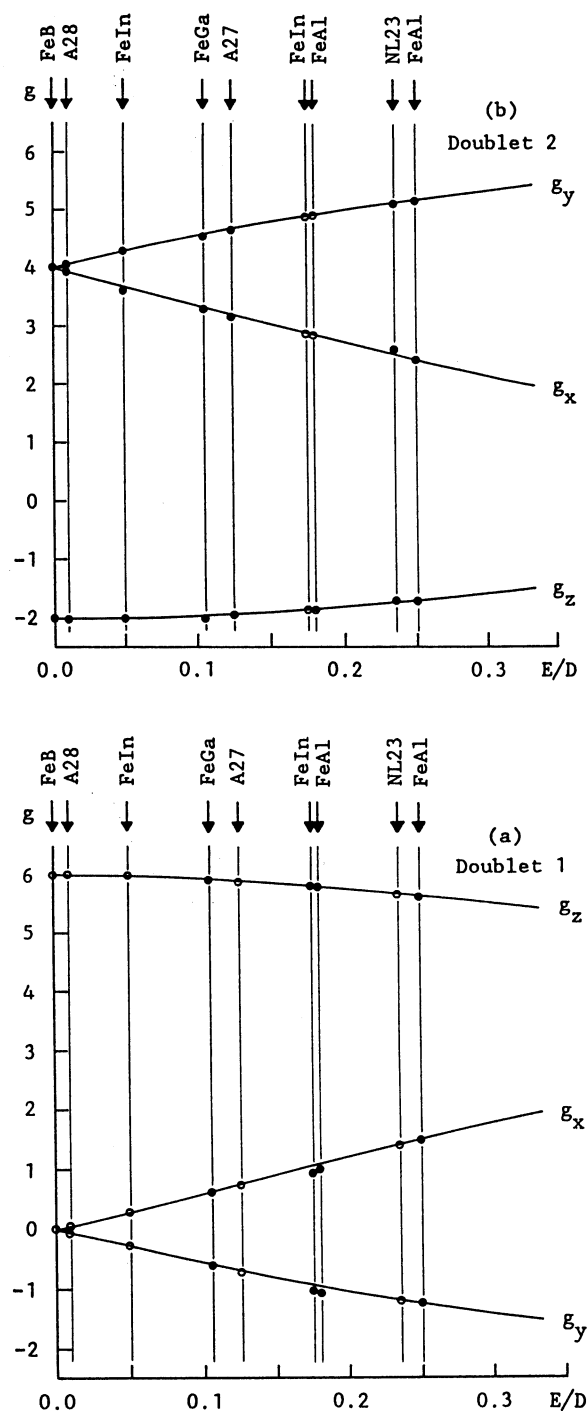


FIGURE 10
Principal g -values (g_x , g_y and g_z) in the two doublets of a true spin $S=3/2$ system. (a) Doublet 1, (b) doublet 2. Solid curves are calculated; experimentally measured data points for nine centres are represented by ●, predicted values by ○.

Table III. Measured and predicted g -values in the spin $S=1/2$ formalism for the three doublets (1, 2 and 3) of a true spin $5/2$ system. g -Values predicted on the basis of the theory are shown in parenthesis.

Centre	Principal g -values			Scale-factor	Scaled g -values			Dou-blet	E/D
	g_1	g_2	g_3		g_1	g_2	g_3		
$Fe_i Fe_i$ mono- clinic	1.15	2.06	9.44	1.035	1.111	1.990	9.121	1	0.205
	3.90	3.50	5.07		3.768	3.382	4.899	2	
	(10.24)	(0.32)	(0.26)		(9.895)	(0.309)	(0.251)	3	
$Fe_i Fe_i B_s$ mono- clinic	1.472	8.899	2.895	1.035	1.422	8.598	2.797	1	0.15
	2.96	3.05	5.46		2.860	3.382	5.275	2	
	(10.29)	(0.17)	(0.14)		(9.947)	(0.161)	(0.139)	3	
$Fe_i Fe_i B_s$ ortho- rhombic	7.902	1.811	4.184	1.035	7.635	1.750	4.043	1	0.08
	1.73	1.94	5.80		1.671	1.874	5.604	2	
	(10.34)	(0.05)	(0.04)		(9.989)	(0.044)	(0.041)	3	
NL20	2.059	6.235	6.235	1.035	1.989	6.024	6.024	1	0.00
	(6.21)	(0.00)	(0.00)		(6.000)	(0.000)	(0.000)	2	
	(10.35)	(0.00)	(0.00)		(10.000)	(0.000)	(0.000)	3	
NL21	4.90	7.38	1.961	1.035	4.734	7.130	1.895	1	0.05
	(6.12)	(1.24)	(1.18)		(5.913)	(1.199)	(1.142)	2	
	(10.34)	(0.02)	(0.02)		(9.994)	(0.017)	(0.016)	3	

be made of the g -values to be expected in the other doublet. These data are as well indicated in figure 10 (on the basis of $g=2$) and in table II (before and after rescaling). Observation in this other doublet may be more difficult due to low Boltzmann occupation of the excited states, or due to an unfavourable g -value. Very low g -values require very strong fields, possibly not experimentally attainable. Other g -values, like $g=6$ give a resonance in a field region which is not commonly carefully scanned, so that these are easily overlooked. Among the trigonal iron-acceptor centres only FeB behaves normally with its $E/D=0$. Trigonal pair FeGa does not satisfy the criteria at all. The two remaining pairs FeAl and FeIn can very well be fitted by the theory, however, with non-zero values for E/D . This has been explained earlier assuming Jahn-Teller distortion of these centres to lower orthorhombic symmetry, but observation of the

centres under motionally averaged conditions, simulating trigonal symmetry⁶. A probably better description is achieved by including orbital motion. In a centre of the relatively high trigonal symmetry not all orbital momentum must be quenched. An analysis on this basis has been given for the trigonal centres²⁶. The present analysis is successful, at least for the monoclinic and orthorhombic centres. Compared to the analysis with spin $S=1/2$ the present analysis has the advantages that (1) a better fit of the angular dependence of the experiment by the theory is obtained, (2) a physically more correct g -value near $g=2$ is used, (3) information on the crystal fields to which the centres are exposed is obtained by determination of E/D and (4) the spin value $S=3/2$ is confirmed to be the physically significant one for these centres. The disadvantage of this analysis is of more practical nature. Whereas the spin $S=1/2$ analy-

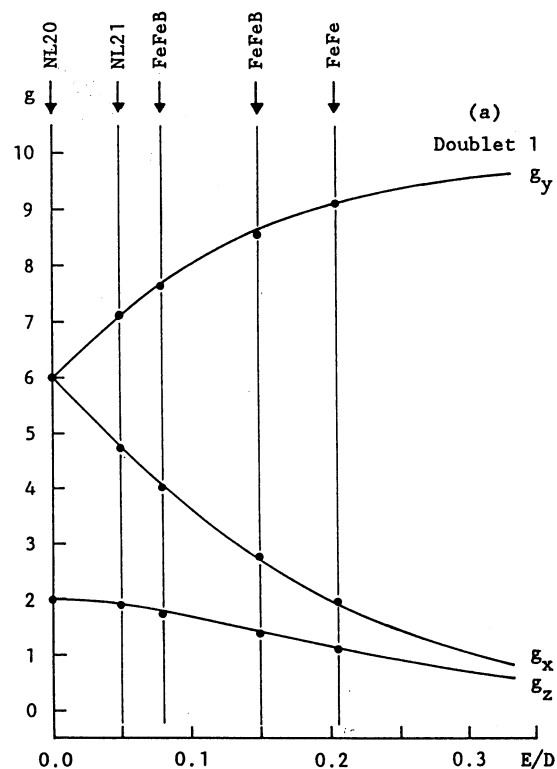
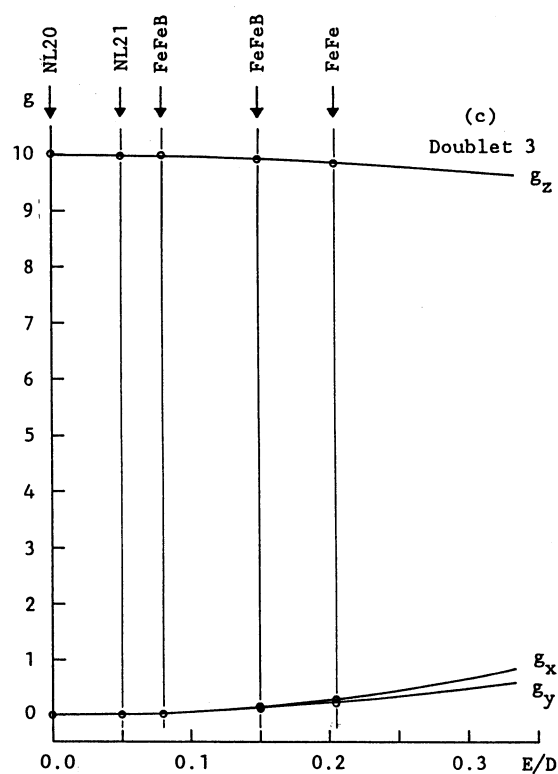
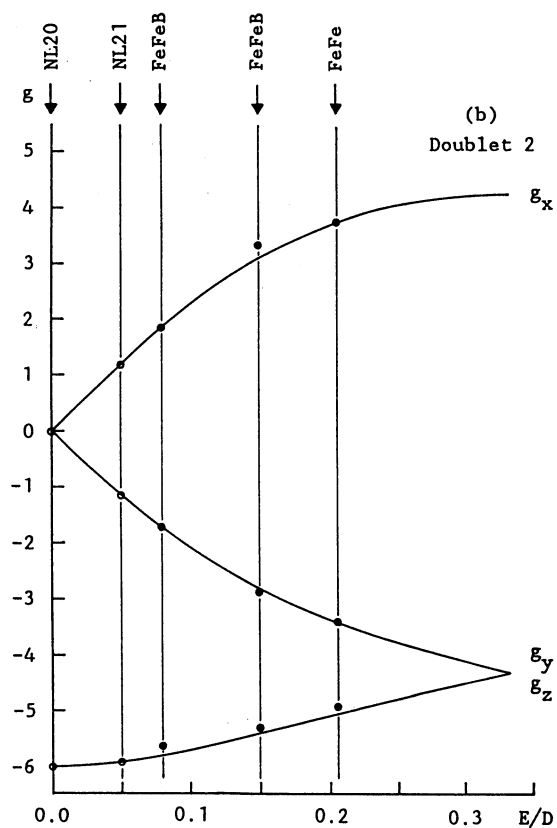


FIGURE 11

Principal g -values (g_x , g_y and g_z) in the three doublets of a true spin $S=5/2$ system. (a) Doublet 1, (b) doublet 2, (c) doublet 3. Solid curves are calculated; experimentally measured data points for five centres are represented by \bullet , predicted values by \circ .

sis uniquely gives best-fit parameters for a well-defined g -tensor, in the $S=3/2$ analysis there is some ambiguity. Changes in E/D can be compensated by changes in g -values, rendering the analysis less straightforward and unique. For centre NL24 a somewhat detailed discussion is given in reference 14. The spin $S=3/2$ established for these centres indicates the presence of three spin-coupled electrons, configuration $3d^3$, or three holes, configuration $3d^7$. The latter configuration is entirely consistent with a positively charged iron atom on an interstitial site, Fe_1^+ , forming part of the centre. Thus the spin is related to a centre with one iron atom in a positive charge state.

3.3 Centres with two iron atoms

For some of the centres a g-value according to equation (7) higher than 2 was calculated, see table I. The centres are $Fe_i Fe_i$ (NL24), the monoclinic and orthorhombic $FeFeB$ -complexes, NL20 and NL21. The high g-value suggests higher spin arising from more electrons. The more detailed analysis for spin $S=5/2$ was presented elsewhere²⁷. Results for this case are summarised in table III and in figure 11. A constant scaling factor 1.035 was assumed. Again, an excellent agreement is observed for the 5 centres in this category. All centres are observable in doublet 1, which apparently is the ground state. Doublet 2 is the intermediate state. Predictions for the g-values of so far unobserved resonances are included in table III and figure 11.

REFERENCES

1. L.S. Vlasenko, A.A. Lebedev, E.S. Tapygov and V.A. Khramtsov, *Sov. Tech. Phys. Lett.* 13 (1987) 553.
2. L.S. Vlasenko, N.T. Son, A.B. van Oosten, C.A.J. Ammerlaan, A.A. Lebedev, E.S. Tapygov and V.A. Khramtsov, *Solid State Commun.*, in print.
3. H.H. Woodbury and G.W. Ludwig, *Phys. Rev.* 126 (1962) 466.
4. G.W. Ludwig and H.H. Woodbury, *Phys. Rev.* 113 (1959) 1014.
5. G.W. Ludwig and H.H. Woodbury, *Electron spin resonance in semiconductors*, in: *Solid State Physics*, Vol. 13, eds. F. Seitz and D. Turnbull (Academic, New York, 1962) pp. 223-304.
6. J.J. van Kooten, G.A. Weller and C.A.J. Ammerlaan, *Phys. Rev. B* 30 (1984) 4564.
7. W. Gehlhoff, K. Irmscher and J. Kreissl, *Electronic properties of pairs of shallow acceptors with iron or manganese in silicon*, in: *New Developments in Semiconductor Physics*, eds. G. Ferenczi and F. Belezny (Springer, Berlin, 1988) pp. 262-267.
8. P. Omling, P. Emanuelsson and H.G. Grimmeiss, *Materials Science Forum* 38-41 (1989) 445.
9. P. Omling, P. Emanuelsson, W. Gehlhoff and H.G. Grimmeiss, *Solid State Commun.* 70 (1989) 807.
10. W. Gehlhoff and K.H. Segsa, *Phys. Stat. Sol. (b)* 115 (1983) 443.
11. G.W. Ludwig and H.H. Woodbury, *Phys. Rev.* 117 (1960) 1286.
12. L.V.C. Assali and J.R. Leite, *Materials Science Forum* 38-41 (1989) 409.
13. A. Chantre and D. Bois, *Phys. Rev. B* 31 (1985) 7979.
14. J.J. van Kooten, E.G. Sieverts and C.A.J. Ammerlaan, *Solid State Commun.* 64 (1987) 1489.
15. W. Gehlhoff, K. Irmscher and U. Rehse, *Materials Science Forum* 38-41 (1989) 373.
16. W. Gehlhoff and U. Rehse, *Solid State Phenomena* 6-7 (1989) 257.
17. S.H. Muller, G.M. Tuynman, E.G. Sieverts and C.A.J. Ammerlaan, *Phys. Rev. B* 25 (1982) 25.
18. C.A.J. Ammerlaan, *Paramagnetic centers in silicon*, in: *Landolt-Börnstein, New series*, Vol. III/22b, ed. M. Schulz (Springer, Berlin, 1989) pp. 365-381.
19. H. Dietrich, H. Vollmer and R. Labusch, *Solid State Commun.* 58 (1986) 811.
20. D. Rodewald, S. Severitt, H. Vollmer and R. Labusch, *Solid State Commun.* 67 (1988) 573.
21. A.B. van Oosten, N.T. Son, L.S. Vlasenko and C.A.J. Ammerlaan, *Materials Science Forum* 38-41 (1989) 355.
22. R. Czaputa, *Appl. Phys. A* 49 (1989) 431.
23. H.J. von Bardeleben, D. Stiévenard, M. Brousseau and J. Barrau, *Phys. Rev. B* 38 (1988) 6308.
24. J.W. Corbett, private communication, 1983.
25. G.W. Ludwig and H.H. Woodbury, *Phys. Rev. Lett.* 1 (1958) 295.
26. C.A.J. Ammerlaan and J.J. van Kooten, *Electronic ground state of iron-acceptor pairs in silicon*, in: *Microscopic Identification of Electronic Defects in Semiconductors*, eds. N.M. Johnson, S.G. Bishop and G.D. Watkins (Materials Research Society, Pittsburgh, 1985) pp. 525-531.
27. C.A.J. Ammerlaan, *Solid State Phenomena* 6-7 (1989) 591.